




2-deoxy-2-[¹⁸F]fluoro-D-glucose Positron Emission Tomography to Monitor Lung Inflammation and Therapeutic Response to Dexamethasone in a Murine Model of Acute Lung Injury

Philip Z. Mannes^{1,2} · Clayton E. Barnes¹ · Joseph D. Latoche³ · Kathryn E. Day³ · Jessie R. Nedrow^{1,3} · Janet S. Lee⁴ · Sina Tavakoli^{1,3,5} 

Received: 25 October 2022 / Revised: 30 January 2023 / Accepted: 7 March 2023 / Published online: 20 March 2023
© The Author(s), under exclusive licence to World Molecular Imaging Society 2023

Abstract

Purpose To image inflammation and monitor therapeutic response to anti-inflammatory intervention using 2-deoxy-2-[¹⁸F]fluoro-D-glucose ([¹⁸F]FDG) positron emission tomography (PET) in a preclinical model of acute lung injury (ALI).

Procedures Mice were intratracheally administered lipopolysaccharide (LPS, 2.5 mg/kg) to induce ALI or phosphate-buffered saline as the vehicle control. A subset of mice in the ALI group received two intraperitoneal doses of dexamethasone 1 and 24 h after LPS. [¹⁸F]FDG PET/CT was performed 2 days after the induction of ALI. [¹⁸F]FDG uptake in the lungs was quantified by PET (%ID/mL_{mean} and standardized uptake value (SUV_{mean})) and *ex vivo* γ -counting (%ID/g). The severity of lung inflammation was determined by quantifying the protein level of inflammatory cytokines/chemokines and the activity of neutrophil elastase and glycolytic enzymes. In separate groups of mice, flow cytometry was performed to estimate the contribution of individual immune cell types to the total pulmonary inflammatory cell burden under different treatment conditions.

Results Lung uptake of [¹⁸F]FDG was significantly increased during LPS-induced ALI, and a decreased [¹⁸F]FDG uptake was observed following dexamethasone treatment to an intermediate level between that of LPS-treated and control mice. Protein expression of inflammatory biomarkers and the activity of neutrophil elastase and glycolytic enzymes were increased in the lungs of LPS-treated mice versus those of control mice, and correlated with [¹⁸F]FDG uptake. Furthermore, dexamethasone-induced decreases in cytokine/chemokine protein levels and enzyme activities correlated with [¹⁸F]FDG uptake. Neutrophils were the most abundant cells in LPS-induced ALI, and the pattern of total cell burden during ALI with or without dexamethasone therapy mirrored that of [¹⁸F]FDG uptake.

Conclusions [¹⁸F]FDG PET noninvasively detects lung inflammation in ALI and its response to anti-inflammatory therapy in a preclinical model. However, high [¹⁸F]FDG uptake by bone, brown fat, and myocardium remains a technical limitation for quantification of [¹⁸F]FDG in the lungs.

Keywords Acute lung injury · [¹⁸F]FDG · Positron emission tomography · Inflammation

✉ Sina Tavakoli
sit23@pitt.edu

¹ Department of Radiology, University of Pittsburgh, Pittsburgh, PA, USA

² Medical Scientist Training Program, University of Pittsburgh, Pittsburgh, PA, USA

³ Department of Medicine, University of Pittsburgh, Pittsburgh, PA, USA

⁴ Division of Pulmonary, Allergy, and Critical Care Medicine, Department of Medicine, University of Pittsburgh, Pittsburgh, PA, USA

⁵ Heart, Lung, Blood, and Vascular Medicine Institute, University of Pittsburgh Medical Center, Pittsburgh, PA, USA

Introduction

Acute lung injury (ALI), clinically known as acute respiratory distress syndrome (ARDS), represents a life-threatening condition in seriously ill patients characterized by an acute onset of pulmonary infiltrates and impaired oxygenation. ARDS is an inflammatory driven disease resulting from direct (e.g., pneumonia) or indirect (e.g., sepsis or trauma) pulmonary insults leading to disruption of the alveolar-capillary barrier and, ultimately, impaired lung function [1]. Clinically, ARDS continues to significantly burden healthcare settings [2], particularly intensive care units, with the incidence of ARDS increasing many folds during the COVID-19 pandemic [3]. Despite our improved understanding on the risk factors that are associated with the development of ARDS, the diagnosis of ARDS remains clinical being based on a constellation of clinical, physiological, and radiographic findings, and we currently lack effective methods to predict patient's outcomes and monitor treatment response.

A promising method for *in vivo* monitoring of molecular patterns of lung inflammation and response to therapy is positron emission tomography (PET). In particular, PET visualizes and quantifies ongoing molecular processes and therefore supplements the anatomical and structural information provided by other imaging modalities, such as computed tomography (CT). Additionally, PET has many advantages to study pulmonary inflammation in comparison to those of currently employed methods. For instance, PET, in contrast to lung biopsy or bronchoalveolar lavage (BAL), noninvasively visualizes lung inflammation without being subject to sampling bias [4]. Moreover, PET may detect molecular patterns of inflammation or resolution at an earlier stage than that of other imaging techniques, including CT [5]. Also, PET is a quantitative technique that is less affected by patient's effort, which represents a major disadvantage of physiological tests, such as pulmonary function tests [6]. Further, PET can be tailored to monitor individual molecular targets or pathways of interest by the use of specific radiotracers. While much effort is currently being devoted to the development of PET tracers targeting specific aspects of the inflammatory response, the most widely available and studied radiotracer remains 2-deoxy-2- ^{18}F fluoro-D-glucose (^{18}F FDG).

Cellular uptake of ^{18}F FDG closely reflects glucose uptake as both ^{18}F FDG and glucose are internalized and processed by related cellular processes [7, 8]. ^{18}F FDG is transported into metabolically active cells via the glucose transporter (GLUT) family of proteins and is subsequently phosphorylated by hexokinases into ^{18}F FDG-6-phosphate, which is essentially irreversibly trapped intracellularly and cannot be further metabolized via glycolysis [9].

Although ^{18}F FDG is most extensively utilized for oncological purposes to detect the tumor-associated Warburg effect, the applications of ^{18}F FDG PET in inflammatory diseases have increased [10–12]. In the inflammatory environment, molecular signals and cascades alter immune cell metabolism in highly orchestrated ways, referred to as immunometabolism. One of the key cellular responses to inflammation is increased glucose metabolism [13]. Given that several cell types abundant in the acutely injured lung, such as neutrophils and macrophages, demonstrate increased influx and glucose metabolism in inflamed tissues, ^{18}F FDG PET is a clinically available method to sensitively and non-invasively visualize *in vivo* changes in glucose metabolism, ultimately a proxy for total inflammatory cell burden [5, 14, 15].

Clinically, ^{18}F FDG PET has been demonstrated to non-invasively monitor the underlying inflammatory processes in various pulmonary diseases. Lung uptake of ^{18}F FDG is increased in chronic obstructive pulmonary disease (COPD), cystic fibrosis, asthma, interstitial lung diseases, and ARDS [11, 14, 16–21]. Importantly, ^{18}F FDG PET provides clinically useful information about disease phenotypes and treatment response. In both COPD [17–19] and idiopathic pulmonary fibrosis [20], for instance, increased ^{18}F FDG uptake correlates with clinical markers of disease severity and indicates aggressive disease status. A separate study has demonstrated that both total and rate of ^{18}F FDG uptake are increased in patients with cystic fibrosis compared to healthy controls, and ^{18}F FDG uptake correlates with neutrophil content of BAL samples [21]. Increased lung uptake of ^{18}F FDG has also been reported in healthy volunteers instilled with intrabronchial endotoxin [11]. Interestingly, ^{18}F FDG PET has been shown to sensitively detect the lung-specific responses to therapies, including statins and recombinant activated protein C, in healthy volunteers receiving intrabronchial endotoxin [14]. While almost all immune and non-immune cells contribute to the total uptake of ^{18}F FDG in the tissues, neutrophils have been shown to have the highest *ex vivo* uptake of ^3H deoxyglucose among the cells recovered by BAL [11, 21].

Despite significant interest in exploring ^{18}F FDG as a method to noninvasively monitor lung inflammation, with a particular interest in improving our ability to molecularly endotype and stratify patients for improving clinical outcomes, there remain critical gaps in our knowledge that limit the interpretation of ^{18}F FDG PET and its utility for understanding lung diseases. Two key gaps include whether ^{18}F FDG uptake correlates with lung tissue expression of inflammatory biomarkers and if ^{18}F FDG can monitor the response to corticosteroids, as a clinically relevant anti-inflammatory therapy in ARDS. In this study, we demonstrated in a preclinical lipopolysaccharide (LPS)-induced

ALI model that [^{18}F]FDG PET noninvasively detected lung inflammation and response to dexamethasone therapy. Additionally, we showed that [^{18}F]FDG uptake correlated with the expression of selected inflammatory proteins and activity of neutrophil elastase and glycolytic enzymes. We further showed that the total number of cells in the lungs, predominantly driven by changes in neutrophils, closely mirrored that of [^{18}F]FDG uptake under different conditions.

Methods

Chemicals and Reagents

The major chemicals and reagents are listed in Supplemental Tables 1–5.

Mouse Model of Experimental Lung Injury

Animal experiments were performed using C57BL/6 J mice (9- to 12-week-old, Jackson Laboratory, strain #000664). Mice were administered intratracheally with 2.5 $\mu\text{g}/\text{g}$ LPS from *Escherichia coli* O111:B4 in 60 μl of phosphate-buffered saline (PBS) to induce lung injury. Control mice were intratracheally injected with 60 μl of PBS. In experiments involving anti-inflammatory treatment, mice received two doses of dexamethasone (10 mg/kg in 500 μl of PBS) via intraperitoneal injections at 1 and 24 h following LPS instillation, whereas non-dexamethasone treated mice were given intraperitoneal PBS (500 μl) injections. Studies were performed in accordance with a protocol approved by the University of Pittsburgh Institutional Animal Care and Use Committee.

PET/CT and Quantification of [^{18}F]FDG Uptake

Mice ($n=4$ PBS, 8 LPS, and 8 LPS + Dexamethasone) were fasted the night prior to PET/CT. Two days after intratracheal LPS or PBS instillation, mice were injected intravenously with [^{18}F]FDG (7.52 ± 0.03 MBq) while awake, and the mice remained awake until PET/CT acquisition. Mice were anesthetized with inhalational isoflurane and static PET (~5-min) and CT (180 projections, 140-ms exposure, 180° rotation, 80-kVp, 500- μA , field-of-view: 78.5×100 -mm) were performed (Inveon, Siemens) ~60 min after radiotracer injection.

Regions of interest were drawn over the left and right lungs, and [^{18}F]FDG uptake in the left and right lungs was averaged and quantified as the mean percentage of injected dose per milliliter of tissue ($\%ID/\text{mL}_{\text{mean}}$) and standard uptake value (SUV_{mean}) (IRW software). The peripheral regions of the lungs were excluded from the regions of interest to minimize the effect of scattered radiation from [^{18}F]

FDG uptake by myocardium and bones. Following PET/CT, mice were euthanized, and radiotracer uptake was also quantified *ex vivo* by γ -counting (Wizard², PerkinElmer) of harvested lungs. Decay-corrected [^{18}F]FDG uptake values are reported.

Lung Homogenization

Following γ -counting, the lungs were frozen at -20 °C and stored for > 10 half-lives to allow [^{18}F]FDG to fully decay. Then, the left lung was mechanically homogenized in 1 mL of distilled water. A 10 \times cytokine lysis buffer (Table S2) was added to the lung homogenate (9 parts of lung homogenate: 1 part of 10 \times cytokine lysis buffer, by volume). After incubating for 30 min at 4 °C, the lung homogenate was centrifuged (10,000 g for 20 min). The resulting supernatant was collected and stored at -80 °C until use.

Protein Expression Assays

The protein expression of select inflammatory markers in the lung homogenate was quantified using an enzyme-linked immunosorbent assay (ELISA) according to the manufacturer's directions (Table S3).

Neutrophil Elastase Activity Assay

The neutrophil elastase activity in lung homogenates was determined as previously described, with minor modifications [22, 23]. Briefly, lung homogenate (10 μL) was incubated with 100 μM of a fluorogenic neutrophil elastase substrate (MeOSuc-AAPV-AMC, Millipore Sigma) in 50 μL assay buffer (100 mM Tris-HCl, 500 mM NaCl, pH = 8.0) at 37 °C. Over the course of 3 h, the fluorescence of each sample was measured every 10 min (Excitation = 380 nm, Emission = 460 nm) with a Synergy H4 Hybrid Microplate Reader (BioTek). The neutrophil elastase activity was calculated as the slope of the linear portion of the fluorescence versus time graph normalized to the average of that of the control mice.

Glycolytic Enzyme Activity Assays

The activity of hexokinase (HK) [24] and lactate dehydrogenase (LDH) [25] was measured using previously reported methods with optimization for use with lung homogenate. Briefly, lung homogenate samples (4.0 μL) were incubated at room temperature with 56.0 μL of the appropriate assay buffers (Tables S3 and S4). The absorbance of each sample, resulting from NADH or NADPH reduction of nitro blue tetrazolium chloride, was measured over 10 min at 1 min intervals at 490 nm [26] using a Synergy H4 Hybrid Microplate Reader (BioTek). The rate of enzymatic activities was

determined as the slope of the linear portion of the absorbance versus time graph normalized to the average of that of the control mice.

Flow Cytometric Immunophenotyping of Murine Lungs

Separate groups of mice treated with LPS ($N=4$), LPS+Dexamethasone ($N=4$), or PBS ($N=4$) were euthanized, and the pulmonary circulation was perfused with PBS via a right ventricular puncture. Both lungs were then minced with scissors and diluted with dissociation buffer (collagenase A, 1.0 mg/mL in PBS supplemented with 1 mM of Ca^{+2} and Mg^{+2}). The lungs were enzymatically dissociated at 37 °C for 1 h with shaking. Then, the resulting cell suspensions were passed through 40- μm cell strainers. After red blood cell lysis, Precision Count Beads (50 μL) were added to each sample. After washing with PBS, cells were incubated with 1% bovine serum albumin (BSA) in PBS and treated first with mouse Fc block (2.0 μL per sample), followed by a mixture of antibodies (0.5 μL per antibody per sample) and DAPI (5.0 μL of 1 $\mu\text{g}/\text{mL}$ per sample) for 0.5 h at 4 °C. Finally, cells were washed and fixed with 4% formalin for 0.5 h at room temperature. Flow cytometry was performed the following day using a LSR II Flow Cytometry (BD Biosciences) and analyzed using FlowJo software version 10.7.2 (BD Biosciences). A list of the antibodies used in this study is available in Table S1.

Statistics

Statistical analysis was performed with Prism 9 (GraphPad). The data are shown as the mean \pm SEM. A one-way analysis of variance, followed by Fisher's Exact post hoc test, was used to compare mean values in > 2 groups. Pearson correlations were used to determine the linear relationship between two variables. Statistical significance was considered as $P < 0.05$.

Results

Noninvasive Detection of ALI and Anti-inflammatory Response to Dexamethasone by [^{18}F]FDG PET

At 1-h post-injection of [^{18}F]FDG, we observed increased radiotracer uptake in the lungs of LPS-treated mice as compared to those of control mice (Fig. 1). The mice receiving LPS followed by dexamethasone demonstrated less lung [^{18}F]FDG uptake than that of LPS-treated mice alone, but greater than that of the control mice. Quantification of PET-derived [^{18}F]FDG uptake confirmed that LPS-treated mice demonstrated significantly increased tracer uptake over PBS-treated mice (by both PET-derived $\%ID/\text{mL}_{\text{mean}}$ and SUV_{mean}), which was significantly reduced by administration of dexamethasone (PET-derived $\%ID/\text{mL}_{\text{mean}}$) with a trend towards a significant decline as measured by SUV_{mean} (Fig. 2A, B).

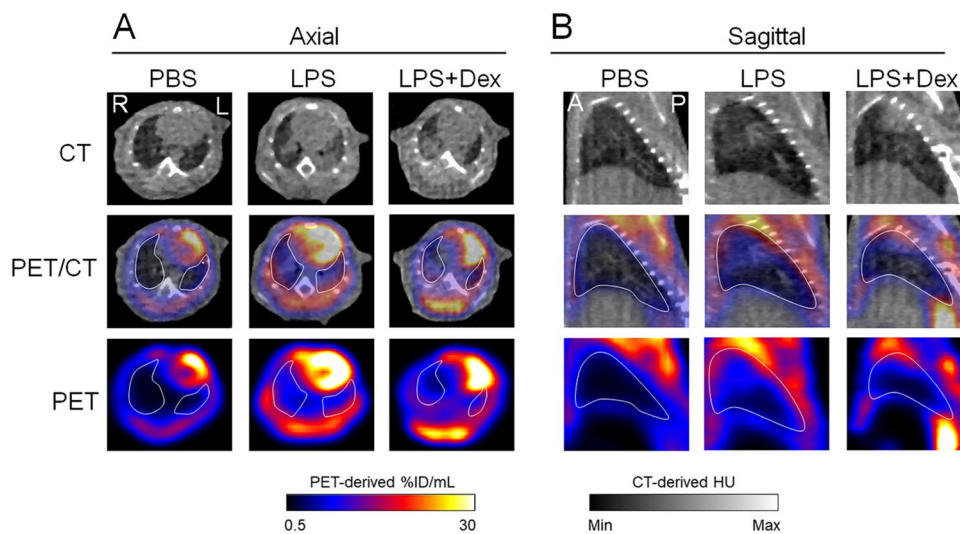
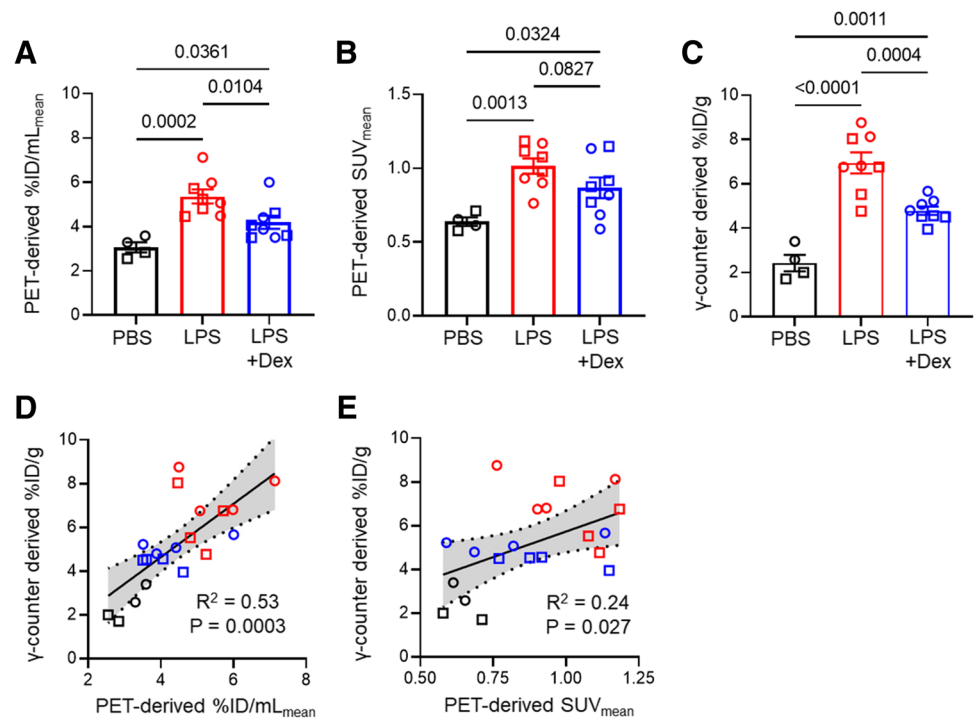


Fig. 1 Representative [^{18}F]FDG PET/CT images in LPS-induced ALI and its response to dexamethasone treatment. (A) Axial and (B) sagittal PET, CT, and coregistered PET/CT images for mice treated with PBS, LPS, or LPS followed by dexamethasone. Mice treated with LPS show focal regions of pulmonary consolidation and groundglass opacities on the CT, which demonstrate increased [^{18}F]FDG uptake. Dexamethasone treatment decreases lung [^{18}F]FDG uptake, although

not to the level of control treated mice. High [^{18}F]FDG uptake is seen in lung-adjacent tissues, including the heart, ribs, and brown fat. The lungs are outlined in white in the PET/CT overlaid images. The white letters indicate image direction: A = anterior, L = left, P = posterior, R = right. Abbreviations: PBS = phosphate-buffered saline, LPS = lipopolysaccharide, Dex = dexamethasone

Fig. 2 Quantification of [^{18}F]FDG uptake in a preclinical LPS-induced ALI model confirms dexamethasone treatment response may be detected noninvasively by [^{18}F]FDG PET. The *in vivo* uptake of [^{18}F]FDG in the lungs was quantified by PET-derived (A) %ID/mL_{mean} and (B) SUV_{mean}. (C) *Ex vivo* γ -counting was performed on the lungs following completion of PET/CT. (D, E) Correlations between *in vivo* and *ex vivo* [^{18}F]FDG uptake were calculated. $N=4$ PBS, 8 LPS, and 8 LPS + Dex treated mice. Equal numbers of male (squares) and female (circles) mice were used per group. Colors: PBS = black, LPS = red, LPS + Dex = blue. Abbreviations: PBS = phosphate-buffered saline, LPS = lipopolysaccharide, Dex = dexamethasone



Ex vivo Quantification of [^{18}F]FDG Uptake by γ -counting Correlates Moderately with PET-derived %ID/mL_{mean}, but Less Strongly with SUV_{mean}

PET-derived quantification of the uptake of radiotracers is subject to inaccuracies resulting from lung-specific (e.g. respiratory motion and lung tissue density) [27, 28] and PET-specific (e.g. scatter, partial volume effect, and positron range) [29, 30] factors. Therefore, we determined the correlations between PET-derived [^{18}F]FDG uptake (%ID/mL_{mean} or SUV_{mean}) in the lung and the uptake quantified by *ex vivo* γ -counting (%ID/g), the gold standard for quantification of radiotracer uptake by organs in preclinical studies, to address the accuracy of *in vivo* quantification of [^{18}F]FDG. Similar to the [^{18}F]FDG uptake determined by PET imaging, mice treated with LPS demonstrated significantly increased [^{18}F]FDG uptake in the lungs, compared to that of control mice by *ex vivo* γ -counting ($6.95\% \pm 0.48$ vs. $2.43\% \pm 0.37$, respectively; $P < 0.0001$) (Fig. 2C). Consistent with PET-derived quantification, mice receiving LPS followed by dexamethasone had an intermediate level of [^{18}F]FDG uptake that was less than that of the LPS only treated mice ($4.79\% \pm 0.19$ vs. $6.95\% \pm 0.48$, respectively; $P = 0.0004$) yet greater than that of the control mice ($4.79\% \pm 0.19$ vs. $2.43\% \pm 0.37$, respectively; $P = 0.0011$). Importantly, there was a moderate correlation between *in vivo* PET-derived %ID/mL_{mean} and *ex vivo* γ -counting-derived (%ID/g) [^{18}F]FDG lung uptake ($R^2 = 0.53$; $P = 0.0003$) (Fig. 2D, E). However, the correlation between *in vivo* PET-derived

SUV_{mean} and *ex vivo* γ -counting-derived (%ID/g) [^{18}F]FDG uptake was less strong ($R^2 = 0.24$; $P = 0.027$).

[^{18}F]FDG Uptake Correlates with Inflammatory Biomarkers and the Activity of Glycolytic Enzymes

One of the hallmarks of experimental ALI is the inflammatory response that is characterized by an increase in cytokines and chemokines [31]. We tested whether increased [^{18}F]FDG lung uptake in ALI correlates with the abundance of select inflammatory proteins. We found that LPS treatment significantly increased the pulmonary expression of pro-inflammatory cytokines and chemokines [1, 32–35], including interleukin 1-beta (IL-1 β), interferon gamma (IFN- γ), interleukin 6 (IL-6), and CXC motif chemokine ligand 1 (CXCL1), versus that of control treated mice (Fig. 3A). Additionally, dexamethasone reduced the expression of these cytokines and chemokines to an intermediate level between that of the LPS-treated and control mice. We further established that lung uptake of [^{18}F]FDG, as measured with *in vivo* %ID/mL_{mean} or SUV_{mean} or *ex vivo* %ID/g, generally correlated with the expression of established inflammatory markers (Fig. 3B). In particular, the *ex vivo* [^{18}F]FDG uptake most strongly correlated with inflammatory markers IL-1 β and CXCL1.

Recruitment and activation of neutrophils are key features of the initial inflammatory phase of ALI [31], which are mediated by several chemokines, including CXCL1. We therefore tested if [^{18}F]FDG uptake correlated with neutrophil elastase activity in lung

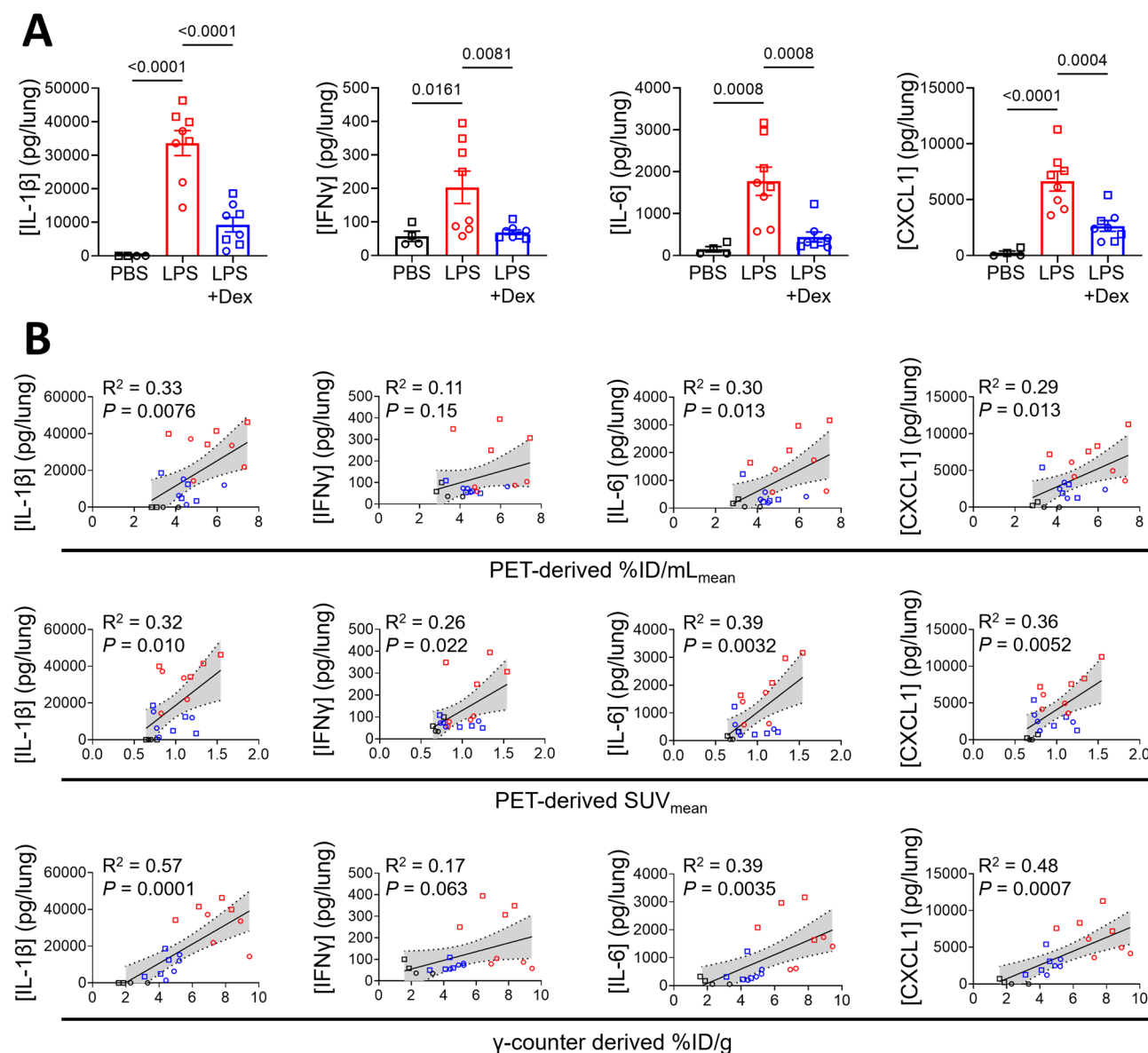


Fig. 3 PET-derived [¹⁸F]FDG uptake correlates with protein expression of inflammatory markers. (A) The protein expression of select markers was determined with an enzyme-linked immunosorbent assay following PET/CT. (B) Expression of inflammatory cytokines/chemokines was correlated with PET-derived (Top: %ID/mL_{mean} or

Middle: SUV_{mean}) and γ-counter-derived (Bottom) [¹⁸F]FDG uptake. *N* = 4 PBS, 8 LPS, and 8 LPS + Dex treated mice. Equal numbers of male (squares) and female (circles) mice were used per group. Abbreviations: PBS = phosphate buffered saline, LPS = lipopolysaccharide, Dex = dexamethasone

homogenate, as a measure for the total burden of neutrophil activation in the lungs [23, 36]. As expected, LPS induced a significant increase in lung neutrophil elastase activity, versus that of control mice, that was decreased upon dexamethasone treatment (Fig. 4A). Although *ex vivo* γ-counting-derived [¹⁸F]FDG uptake correlated with neutrophil elastase activity ($R^2 = 0.43$, $P = 0.0017$), the correlations were weaker with PET-derived quantification of [¹⁸F]FDG uptake (%ID/mL_{mean}: $R^2 = 0.18$, $P = 0.064$ and SUV_{mean}: $R^2 = 0.28$, $P = 0.017$) (Fig. 4B).

As several inflammatory stimuli inhibit the tricarboxylic acid cycle, many leukocytes in inflammatory environments rely on glycolysis for energy production and proper inflammatory functions [37–41]. Further, a switch to glycolysis with an associated increase in lactate production represents a validated metabolic alteration and poor clinical prognostic factor in ARDS [42–49]. We therefore examined whether [¹⁸F]FDG uptake correlates with pulmonary glycolytic activity of HK and LDH. We focused on HK and LDH as they represent important steps in glycolysis; HK traps

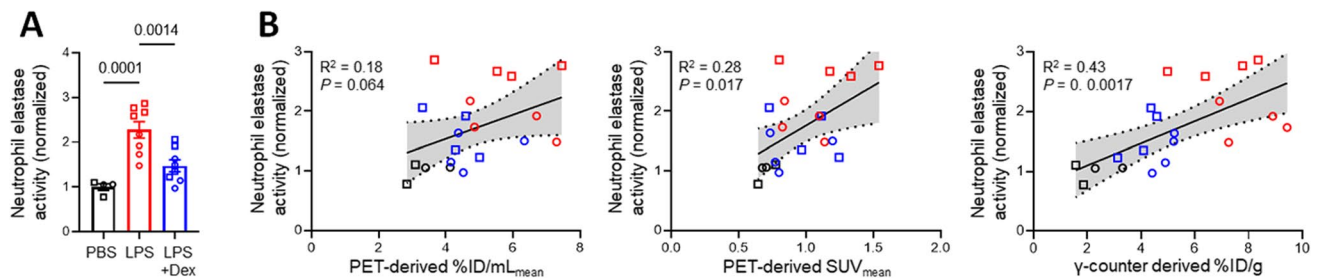


Fig. 4 Pulmonary [^{18}F]FDG uptake correlates with neutrophil elastase activity. **(A)** Neutrophil elastase activity was determined in lung homogenates following PET/CT. The total neutrophil elastase activity is increased following intratracheal instillation of LPS and decreases nearly to baseline with dexamethasone treatment. The neutrophil elastase activity of LPS and LPS+Dex groups was normalized to the average of the controls. **(B)** Neutrophil elastase activity

was correlated with PET-derived (Left: %ID/mL_{mean} or Middle: SUV_{mean}) or γ -counter-derived (Right) [^{18}F]FDG uptake. $N=4$ PBS, 8 LPS, and 8 LPS+Dex treated mice. Equal numbers of male (squares) and female (circles) mice were used per group. Abbreviations: PBS = phosphate buffered saline, LPS = lipopolysaccharide, Dex = dexamethasone

glucose and [^{18}F]FDG intracellularly via phosphorylation whereas LDH catalyzes the critical final step of glycolysis to regenerate NAD⁺ to sustain high levels of glycolysis. Following LPS treatment, we found that the relative activity of HK and LDH were both significantly increased over that of controls (Fig. 5A). Interestingly, dexamethasone decreased HK and LDH activities to the levels of control mice. Further, the HK and LDH activity both generally correlated with [^{18}F]FDG uptake, although most strongly with *ex vivo* γ -counting-derived measurements (Fig. 5B).

Neutrophil Burden in the Lungs Mirrors the Observed Pattern of [^{18}F]FDG Uptake in LPS-induced ALI and Response to Anti-inflammatory Treatment

To determine changes in pulmonary immune cell populations in response to LPS administration with or without dexamethasone treatment, we first determined the absolute cell count for individual cell types harvested from the lungs (Fig. 6A) using a flow cytometry gating strategy provided in Fig. S1. Following LPS-treatment, we detected significantly

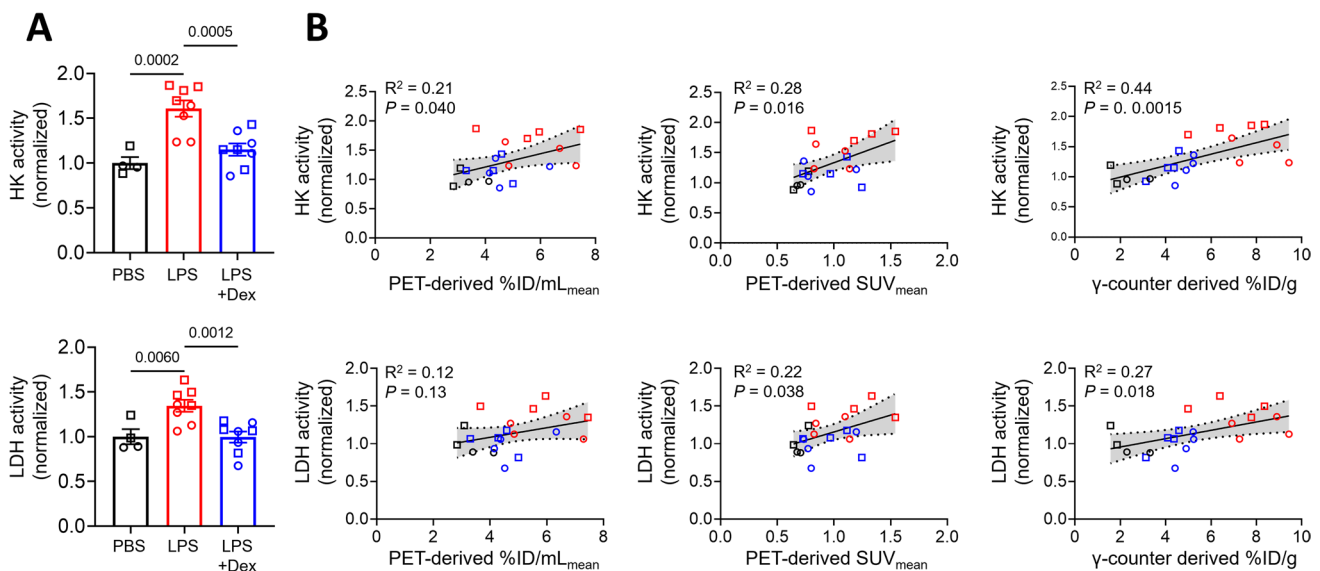


Fig. 5 [^{18}F]FDG uptake correlates with the activity of glycolytic enzymes. **(A)** The activity of hexokinase (HK) and lactate dehydrogenase (LDH) in lung homogenates was measured following PET/CT. The total lung activity of both enzymes was significantly increased following administration of LPS. Anti-inflammatory treatment by dexamethasone reduced the activity of HK and LDH nearly to that of controls. Enzymatic activity was normalized to that of the average of

the controls. **(B)** HK and LDH activities were correlated with PET-derived (Left: %ID/mL_{mean} or Middle: SUV_{mean}) or γ -counter-derived (Right) [^{18}F]FDG uptake. $N=4$ PBS, 8 LPS, and 8 LPS+Dex treated mice. Equal numbers of male (squares) and female (circles) mice were used per group. Abbreviations: PBS = phosphate-buffered saline, LPS = lipopolysaccharide, Dex = dexamethasone

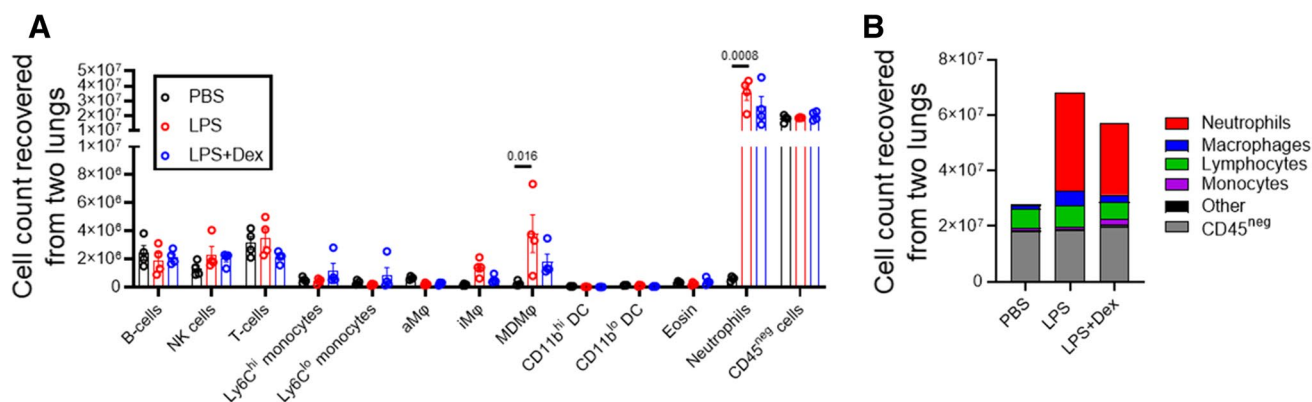


Fig. 6 Neutrophils are the most abundant cell type during LPS-induced ALI as measured by flow cytometry. **(A)** The cell count was quantified for mice treated with intratracheal LPS or LPS + Dex vs. control. **(B)** The relative contribution of individual cell types to the total recovered cells from the lungs of mice following treatment with LPS and/or dexamethasone versus control, as visualized with a stacked-bar graph. Abbreviations: NK cells = natural killer

cells; aMφ = alveolar macrophage; iMφ = interstitial macrophage; MDMφ = monocyte-derived macrophage; CD11b^{hi} DC = CD11b^{hi} dendritic cells; CD11b^{lo} DC = CD11b^{lo} dendritic cells; Eosin = eosinophils; CD45^{neg} cells = non-immune cells. *N* = 4 PBS, 4 LPS, and 4 LPS + Dex treated mice. Equal numbers of male and female mice were used per group. Abbreviations: PBS = phosphate-buffered saline, LPS = lipopolysaccharide, Dex = dexamethasone

increased numbers of lung neutrophils (e.g., ~60-fold increase) versus that of control mice ($P = 0.0008$) (Fig. 6A). However, LPS induced only modest increases in the number of several other lung immune cell populations, including interstitial and monocyte-derived macrophages. We found that dexamethasone treatment reduced the number of infiltrating neutrophils without affecting the abundance of other cell populations. Additionally, we observed minimal changes to the number of lymphoid cells (B-cells, natural killer cells, and T-cells), monocytes (Ly6C^{hi} and Ly6C^{lo}), dendritic cells (CD11b^{hi} and CD11b^{lo}), eosinophils, and CD45^{neg} non-immune cells after treatment with LPS or dexamethasone versus that of controls.

We next calculated the relative contributions of individual cell types to the total pulmonary cell counts under different treatment conditions (Fig. 6B). Unsurprisingly, LPS-treated mice exhibited the highest number of total lung cells, with neutrophils accounting for over half of all cells in the lungs of mice with LPS-induced ALI. Dexamethasone therapy decreased the number of lung leukocytes largely due to a decrease in the number of neutrophils. By contrast, neutrophils represented only 2% of all cells in the control lungs. As the changes in CD45^{neg} cells and other leukocyte populations were relatively minor compared to that of the neutrophils, the change in total cell count was driven primarily by neutrophils. Furthermore, we observed the total cell count measured by flow cytometry in different experimental groups (Fig. 6B) closely mirrored that of [¹⁸F]FDG uptake under the same treatment conditions (Fig. 2). Unsurprisingly, CD45^{neg} cells represent a significant fraction of total lung cells under all conditions and are presumably a major contributor to [¹⁸F]FDG uptake in healthy lungs.

Discussion

In this study, we demonstrate that [¹⁸F]FDG uptake is increased in LPS-induced ALI and noninvasively detects the response to a clinically relevant anti-inflammatory therapy, dexamethasone. We found that [¹⁸F]FDG uptake during ALI with or without dexamethasone treatment correlates with the degree of inflammatory cytokine/chemokine expression and the activity of neutrophil elastase and glycolytic enzymes. We further found that [¹⁸F]FDG uptake closely mirrors the pattern of pulmonary neutrophil accumulation during ALI, the dominant immune cell population in this model. Thus, [¹⁸F]FDG PET is effective in monitoring ongoing and resolving lung inflammation through its correlations with lung specific expression of inflammatory biomarkers and active neutrophils.

While the pathophysiology of ARDS/ALI is complex, we demonstrate that [¹⁸F]FDG PET noninvasively and directly monitors specific aspects of the inflammatory response in the lung that are difficult to obtain via other available techniques. We show that [¹⁸F]FDG uptake correlates with pathogenically relevant and therapeutically targetable biomarkers expressed in lung tissue, which may prove advantageous over measurement of serum biomarkers that may reflect systemic rather than lung specific inflammatory processes. Importantly, we found that [¹⁸F]FDG uptake monitors the anti-inflammatory response to dexamethasone therapy, as confirmed by correlations between reduced radiotracer uptake with decreased expression of inflammatory mediators, including cytokines, chemokines, and proteases. Furthermore, [¹⁸F]FDG PET more accurately visualizes the response to anti-inflammatory treatment compared to that of

CT, as demonstrated by reduced [^{18}F]FDG uptake in regions of CT-defined pulmonary airspace opacification following steroid therapy.

Despite the widespread use of and research on [^{18}F]FDG for imaging inflammation, there remain biologic and technological limitations that may hinder interpretability of [^{18}F]FDG for monitoring lung inflammation. For example, both clinical and preclinical studies have shown that all metabolically active cells metabolize [^{18}F]FDG, including the liver, ribs, heart, and brown fat [50–53]. Due to the positron range and scattered radiation, the high radiotracer uptake in extrapulmonary tissues, enhanced by the systemic inflammation induced by LPS, appears to spillover into the lungs, and leads to overestimation of the true extent of pulmonary [^{18}F]FDG uptake by PET in regions adjacent to organs with high [^{18}F]FDG uptake. In preclinical experiments, the combination of respiratory motion from non-respiratory gated scans and small subject size further enhances the undesirable impact of the relatively high positron range and scattered radiation, ultimately leading to inaccurate assessments of pulmonary radiotracer uptake. These limitations may account for the moderate correlation between *ex vivo* γ -counting (%ID/g) derived [^{18}F]FDG uptake and *in vivo* PET %ID/mL_{mean} and fair correlation between *ex vivo* γ -counting (%ID/g) derived [^{18}F]FDG uptake and *in vivo* PET SUV_{mean}. The lower correlation strength of SUV_{mean} with γ -counting-derived uptake values may result from the weight loss in LPS-treated mice that lowers the SUV_{mean} [54–57]. As the %ID/mL does not account for weight changes, we observed a stronger correlation between PET-derived %ID/mL_{mean} and γ -counting derived %ID/g. Notably, the correlations between [^{18}F]FDG uptake and biological markers in our study were generally strongest when tracer uptake was assessed by *ex vivo* γ -counting, consistent with the inaccuracies of *in vivo* PET-derived measurements. While the larger size of humans and implementation of respiratory gating in clinical scans reduce the above mentioned effects, the non-specific [^{18}F]FDG uptake by the heart, liver, and ribs may obscure inflammatory processes in the lung periphery and subpleural space.

Although [^{18}F]FDG PET is the most popular molecular imaging approach for assessment of inflammation, there remains a clear need to develop new radiotracers targeting specific aspects of the inflammatory process. In particular, our study demonstrates that [^{18}F]FDG uptake is likely driven by abundant, metabolically active cell types, e.g., neutrophils in the case of ALI [4, 10, 11, 58, 59], with probable contributions from lung parenchymal cells. Additionally, prior studies have shown that neutrophils contribute to most [^3H]deoxyglucose uptake among the cells recovered from BAL of humans intrabronchially administered with LPS [11, 21]. To address the non-specificity of [^{18}F]FDG, selective PET agents have been developed to study specific inflammatory

pathways, particularly monocyte/macrophage-driven inflammation. For instance, the PET tracer [^{64}Cu]DOTA-ECL1i is reported to target CCR2-expressing monocytes [60, 61], which have been demonstrated to be relevant in pulmonary inflammation and noninvasively monitors response to immunotherapies. Additionally, we have recently reported that [^{64}Cu]NODAGA-CG34, a PET tracer that selectively binds to chemokine-like receptor-1 (CMKLR1), detects the accumulation of monocyte-derived macrophages in the lungs of mice with ALI [62]. Other emerging molecular imaging targets include, $\alpha_4\beta_1$ integrin [63], leukocyte receptor CD11b [64], folate receptor- β [65], and translocator protein receptor [66], which have been successfully used for noninvasive detection of lung inflammation in ALI.

There remain several limitations of our current study. First, as previously mentioned, the high degree of [^{18}F]FDG uptake in lung-adjacent tissues results in the spillover of radiotracer signal into the lungs, as measured by PET. To minimize the unwanted contribution from these non-lung organs to the lung [^{18}F]FDG uptake, we drew our regions of interest to include a few millimeter margins between the lung and adjacent organs, leading to underestimation of lung radiotracer uptake. Another limitation of our study is that we measured a relatively limited number of inflammatory and glycolytic markers with which to correlate [^{18}F]FDG uptake. We chose to measure these chemokines, cytokines, and enzymes as they are common biomarkers characterizing the inflammatory response observed in experimental ALI [31]. Additionally, decreased blood flow to areas of lung inflammation due to hypoxia-induced vasoconstriction [67] is expected to affect the observed [^{18}F]FDG uptake. Kinetic analysis of [^{18}F]FDG uptake along with perfusion PET imaging allows for a more accurate measurement of the rate of [^{18}F]FDG uptake. However, the static PET design of our approach is aligned with our primary goal to determine the utility of the [^{18}F]FDG PET according to the currently performed clinical protocols to monitor lung inflammation and response to therapy.

In conclusion, [^{18}F]FDG PET may be useful in monitoring ongoing pulmonary inflammation and therapeutic response. Additionally, our data along with the previous publications [11, 21] suggest that [^{18}F]FDG uptake is mostly driven by the metabolic activity of neutrophils in this preclinical model of ALI, and is less reflective of other specific subsets of immune cells. While our results should encourage additional work into better understanding the biological correlations of [^{18}F]FDG uptake, there remains a clear need to develop new radiotracers targeting specific aspects of the inflammatory process and better understand the biologic correlates of molecular imaging.

Supplementary Information The online version contains supplementary material available at <https://doi.org/10.1007/s11307-023-01813-w>.

Acknowledgements This work utilized the Hillman Cancer Center *In vivo* Imaging Facility, a shared resource at the University of Pittsburgh (supported by P30CA047904). Additionally, we would like to thank the Flow Cytometry Core Facility at the University of Pittsburgh.

Funding National Heart, Lung, and Blood Institute grant F30HL158038 (PZM)

National Institute of Biomedical Imaging and Bioengineering grant R21EB027871 (ST)

National Heart, Lung, and Blood Institute grant K08HL144911 (ST)
National Heart, Lung, and Blood Institute grant R01HL136143 (JSL)

National Heart, Lung, and Blood Institute grant P01HL114453 (JSL)

National Heart, Lung, and Blood Institute grant R01HL142084 (JSL)

National Heart, Lung, and Blood Institute grant K24HL143285 (JSL)

National Institutes of Health, Cancer Center Support Grant P30CA047904 (JRN, KD, JDL)

Data Availability The data needed to evaluate the conclusions of the paper are present in the paper and/or the Supplementary Materials.

Declarations

Conflicts of Interest JSL reports personal fees from Janssen R&D, which is outside of the submitted work. No other authors report conflicts of interest.

References

- Matthay MA, Zemans RL, Zimmerman GA et al (2019) Acute respiratory distress syndrome. *Nat Rev Dis Primers* 5:18
- Pham T, Rubenfeld GD (2017) Fifty years of research in ARDS. The epidemiology of acute respiratory distress syndrome. A 50th birthday review. *Am J Respir Crit Care Med* 195:860–870
- Hendrickson KW, Peltan ID, Brown SM (2021) The epidemiology of acute respiratory distress syndrome before and after Coronavirus disease 2019. *Crit Care Clin* 37:703–716
- Musch G, Venegas JG, Bellani G et al (2007) Regional gas exchange and cellular metabolic activity in ventilator-induced lung injury. *Anesthesiology* 106:723–735
- Vass L, Fisk M, Lee S, Wilson FJ, Cheriyan J, Wilkinson I (2020) Advances in PET to assess pulmonary inflammation: a systematic review. *Eur J Radiol* 130:109182
- Barreiro TJ, Perillo I (2004) An approach to interpreting spirometry. *Am Fam Physician* 69:1107–1114
- Pauwels EK, McCready VR, Stoot JH, van Deurzen DF (1998) The mechanism of accumulation of tumour-localising radiopharmaceuticals. *Eur J Nucl Med* 25:277–305
- Gallagher BM, Fowler JS, Guttererson NI, MacGregor RR, Wan CN, Wolf AP (1978) Metabolic trapping as a principle of radiopharmaceutical design: some factors responsible for the biodistribution of [18F] 2-deoxy-2-fluoro-D-glucose. *J Nucl Med* 19:1154–1161
- Barrio JR, Huang SC, Satyamurthy N et al (2020) Does 2-FDG PET accurately reflect quantitative *in vivo* glucose utilization? *J Nucl Med* 61:931–937
- Chen DL, Schuster DP (2004) Positron emission tomography with [18F]fluorodeoxyglucose to evaluate neutrophil kinetics during acute lung injury. *Am J Physiol Lung Cell Mol Physiol* 286:L834–840
- Chen DL, Rosenbluth DB, Mintun MA (1985) Schuster DP (2006) FDG-PET imaging of pulmonary inflammation in healthy volunteers after airway instillation of endotoxin. *J Appl Physiol* 100:1602–1609
- Graebe M, Pedersen SF, Borgwardt L, Hojgaard L, Sillesen H, Kjaer A (2009) Molecular pathology in vulnerable carotid plaques: correlation with [18]-fluorodeoxyglucose positron emission tomography (FDG-PET). *Eur J Vasc Endovasc Surg* 37:714–721
- O'Neill LA, Kishton RJ, Rathmell J (2016) A guide to immunometabolism for immunologists. *Nat Rev Immunol* 16:553–565
- Chen DL, Bedient TJ, Kozlowski J et al (2009) [18F]fluorodeoxyglucose positron emission tomography for lung antiinflammatory response evaluation. *Am J Respir Crit Care Med* 180:533–539
- de Prost N, Tucci MR, Melo MF (2010) Assessment of lung inflammation with 18F-FDG PET during acute lung injury. *AJR Am J Roentgenol* 195:292–300
- Capitanio S, Nordin AJ, Noraini AR, Rossetti C (2016) PET/CT in nononcological lung diseases: current applications and future perspectives. *Eur Respir Rev* 25:247–258
- Subramanian DR, Jenkins L, Edgar R, Quraishi N, Stockley RA, Parr DG (2012) Assessment of pulmonary neutrophilic inflammation in emphysema by quantitative positron emission tomography. *Am J Respir Crit Care Med* 186:1125–1132
- Torigian DA, Dam V, Chen X et al (2013) *In vivo* quantification of pulmonary inflammation in relation to emphysema severity via partial volume corrected (18)F-FDG-PET using computer-assisted analysis of diagnostic chest CT. *Hell J Nucl Med* 16:12–18
- Jones HA, Marino PS, Shakur BH, Morrell NW (2003) *In vivo* assessment of lung inflammatory cell activity in patients with COPD and asthma. *Eur Respir J* 21:567–573
- Yoon HY, Lee SH, Ha S, Ryu JS, Song JW (2021) The value of (18)F-FDG PET/CT in evaluating disease severity and prognosis in idiopathic pulmonary fibrosis patients. *J Korean Med Sci* 36:e257
- Chen DL, Ferkol TW, Mintun MA, Pittman JE, Rosenbluth DB, Schuster DP (2006) Quantifying pulmonary inflammation in cystic fibrosis with positron emission tomography. *Am J Respir Crit Care Med* 173:1363–1369
- Ishii T, Doi K, Okamoto K et al (2010) Neutrophil elastase contributes to acute lung injury induced by bilateral nephrectomy. *Am J Pathol* 177:1665–1673
- Zhao Y, Olonisakin TF, Xiong Z et al (2015) Thrombospondin-1 restrains neutrophil granule serine protease function and regulates the innate immune response during *Klebsiella pneumoniae* infection. *Mucosal Immunol* 8:896–905
- TeSlaa T, Teitell MA (2014) Techniques to monitor glycolysis. *Methods Enzymol* 542:91–114
- Jelinek D, Flores A, Uebelhoer M et al (2018) Mapping metabolism: monitoring lactate dehydrogenase activity directly in tissue. *J Vis Exp* 136:e57760
- Lokuta MA, Mehring GH, Paulnock DM (1997) Spectrophotometric determination of oxidative metabolism. *Biotechniques* 22:841–844
- Chen DL, Ballout S, Chen L et al (2020) Consensus recommendations on the use of (18)F-FDG PET/CT in lung disease. *J Nucl Med* 61:1701–1707
- Chen DL, Cheriyan J, Chilvers ER et al (2017) Quantification of lung PET images: challenges and opportunities. *J Nucl Med* 58:201–207
- Soret M, Bacharach SL, Buvat I (2007) Partial-volume effect in PET tumor imaging. *J Nucl Med* 48:932–945
- Carter LM, Kesner AL, Pratt EC et al (2020) The impact of positron range on PET resolution, evaluated with phantoms and

- PHITS monte carlo simulations for conventional and non-conventional radionuclides. *Mol Imaging Biol* 22:73–84
31. Kulkarni HS, Lee JS, Bastarache JA et al (2022) Update on the features and measurements of experimental acute lung injury in animals: an official American thoracic society workshop report. *Am J Respir Cell Mol Biol* 66:e1–e14
 32. Bos LD, Schouten LR, van Vught LA et al (2017) Identification and validation of distinct biological phenotypes in patients with acute respiratory distress syndrome by cluster analysis. *Thorax* 72:876–883
 33. Famous KR, Delucchi K, Ware LB et al (2017) Acute respiratory distress syndrome subphenotypes respond differently to randomized fluid management strategy. *Am J Respir Crit Care Med* 195:331–338
 34. Reilly JP, Calfee CS, Christie JD (2019) Acute respiratory distress syndrome phenotypes. *Semin Respir Crit Care Med* 40:19–30
 35. Williams AE, Chambers RC (2014) The mercurial nature of neutrophils: still an enigma in ARDS? *Am J Physiol Lung Cell Mol Physiol* 306:L217–230
 36. Qu Y, Olonisakin T, Bain W et al (2018) Thrombospondin-1 protects against pathogen-induced lung injury by limiting extracellular matrix proteolysis. *JCI Insight* 3:e96914
 37. Rodriguez-Prados JC, Traves PG, Cuenca J et al (2010) Substrate fate in activated macrophages: a comparison between innate, classic, and alternative activation. *J Immunol* 185:605–614
 38. Borregaard N, Herlin T (1982) Energy metabolism of human neutrophils during phagocytosis. *J Clin Investig* 70:550–557
 39. Sadiku P, Willson JA, Ryan EM et al (2021) Neutrophils fuel effective immune responses through gluconeogenesis and glycolysis. *Cell Metab* 33(411–423):e414
 40. Kelly B, O'Neill LA (2015) Metabolic reprogramming in macrophages and dendritic cells in innate immunity. *Cell Res* 25:771–784
 41. Tannahill GM, Curtis AM, Adamik J et al (2013) Succinate is an inflammatory signal that induces IL-1 β through HIF-1 α . *Nature* 496:238–242
 42. Beca JP, Scopes JW (1972) Serial determinations of blood lactate in respiratory distress syndrome. *Arch Dis Child* 47:550–557
 43. Zhang H, Li Z, Zheng W et al (2022) Risk stratification of patients with acute respiratory distress syndrome complicated with sepsis using lactate trajectories. *BMC Pulm Med* 22:339
 44. Wu C, Chen X, Cai Y et al (2020) Risk factors associated with acute respiratory distress syndrome and death in patients with Coronavirus disease 2019 pneumonia in Wuhan, China. *JAMA Intern Med* 180:934–943
 45. Sipahioglu H, Onuk S (2022) Lactate dehydrogenase/albumin ratio as a prognostic factor in severe acute respiratory distress syndrome cases associated with COVID-19. *Medicine (Baltimore)* 101:e30759
 46. Alipanah-Lechner N, Neyton L, Mick E et al (2023) Plasma metabolic profiling implicates dysregulated lipid metabolism and glycolytic shift in hyperinflammatory ARDS. *Am J Physiol Lung Cell Mol Physiol* 324:L297–L306
 47. Santos AF, Pova P, Paixao P, Mendonca A, Taborda-Barata L (2021) Changes in glycolytic pathway in SARS-COV 2 infection and their importance in understanding the severity of COVID-19. *Front Chem* 9:685196
 48. Pourfathi M, Cereda M, Chatterjee S et al (2018) Lung metabolism and inflammation during mechanical ventilation. *An Imaging Approach Sci Rep* 8:3525
 49. Robinson MJ, Krasnodembkaya AD (2020) Therapeutic targeting of metabolic alterations in acute respiratory distress syndrome. *Eur Respir Rev* 29:200114
 50. Ledoult E, Morelle M, Soussan M et al (2021) (18)F-FDG positron emission tomography scanning in systemic sclerosis-associated interstitial lung disease: a pilot study. *Arthritis Res Ther* 23:76
 51. Puuvuori E, Liggieri F, Velikyan I et al (2022) PET-CT imaging of pulmonary inflammation using [(68)Ga]Ga-DOTA-TATE. *EJNMMI Res* 12:19
 52. Steinberg JD, Vogel W, Vegt E (2017) Factors influencing brown fat activation in FDG PET/CT: a retrospective analysis of 15,000+ cases. *Br J Radiol* 90:20170093
 53. Long NM, Smith CS (2011) Causes and imaging features of false positives and false negatives on F-PET/CT in oncologic imaging. *Insights Imaging* 2:679–698
 54. Keyes JW Jr (1995) SUV: standard uptake or silly useless value? *J Nucl Med* 36:1836–1839
 55. Weiss GJ, Korn RL (2012) Interpretation of PET scans: do not take SUVs at face value. *J Thorac Oncol* 7:1744–1746
 56. Blau M (1975) Letter: radiation dosimetry of 131-I-19-iodocholesterol: The pitfalls of using tissue concentration data. *J Nucl Med* 16:247–249
 57. Adams MC, Turkington TG, Wilson JM, Wong TZ (2010) A systematic review of the factors affecting accuracy of SUV measurements. *AJR Am J Roentgenol* 195:310–320
 58. Zambelli V, Di Grigoli G, Scanziani M et al (2012) Time course of metabolic activity and cellular infiltration in a murine model of acid-induced lung injury. *Intensive Care Med* 38:694–701
 59. Kubota R, Yamada S, Kubota K, Ishiwata K, Tamahashi N, Ido T (1992) Intratumoral distribution of fluorine-18-fluorodeoxyglucose *in vivo*: high accumulation in macrophages and granulation tissues studied by microautoradiography. *J Nucl Med* 33:1972–1980
 60. Liu Y, Gunsten SP, Sultan DH et al (2017) PET-based imaging of chemokine receptor 2 in experimental and disease-related lung inflammation. *Radiology* 283:758–768
 61. Brody SL, Gunsten SP, Luehmann HP et al (2021) Chemokine receptor 2-targeted molecular imaging in pulmonary fibrosis. A clinical trial. *Am J Respir Crit Care Med* 203:78–89
 62. Mannes PZ, Barnes CE, Biermann J et al (2023) Molecular imaging of chemokine-like receptor 1 (CMKLR1) in experimental acute lung injury. *Proc Natl Acad Sci U S A* 120:e2216458120
 63. Haddad J, Latoche JD, Nigam S et al (2021) Molecular imaging of very late antigen-4 in acute lung injury. *J Nucl Med* 62:280–286
 64. Cao Q, Huang Q, Mohan C, Li C (2019) Small-animal PET/CT imaging of local and systemic immune response using (64)Cu-alphaCD11b. *J Nucl Med* 60:1317–1324
 65. Han W, Zaynagetdinov R, Yull FE et al (2015) Molecular imaging of folate receptor beta-positive macrophages during acute lung inflammation. *Am J Respir Cell Mol Biol* 53:50–59
 66. Hardwick MJ, Chen MK, Baidoo K, Pomper MG, Guilarte TR (2005) *In vivo* imaging of peripheral benzodiazepine receptors in mouse lungs: a biomarker of inflammation. *Mol Imaging* 4:432–438
 67. Antoni G, Lubberink M, Sorensen J et al (2023) *In vivo* visualization and quantification of neutrophil elastase in lungs of COVID-19 patients: a first-in-humans PET study with (11)C-NES. *J Nucl Med* 64:145–148

Publisher's Note Springer Nature remains neutral with regard to jurisdictional claims in published maps and institutional affiliations.

Springer Nature or its licensor (e.g. a society or other partner) holds exclusive rights to this article under a publishing agreement with the author(s) or other rightsholder(s); author self-archiving of the accepted manuscript version of this article is solely governed by the terms of such publishing agreement and applicable law.